Cryogenic X-ray Crystal Structure Analysis for the Complex of Scytalone Dehydratase of a Rice Blast Fungus and Its Tight-Binding Inhibitor, Carpropamid: The Structural Basis of Tight-Binding Inhibition[†,‡]

Masayoshi Nakasako,[§] Takayuki Motoyama,[∥] Yoshio Kurahashi,[⊥] and Isamu Yamaguchi*[,∥]

The Institute of Physical and Chemical Research (RIKEN), Wako, Saitama 351-0198, Japan, Precursory Research for Embryonic Science and Technology (PRESTO), Japan Science and Technology Corporation (JST), and Institute of Molecular and Cellular Biosciences, The University of Tokyo, Bunkyoku, Tokyo 113-0032, Japan, and Yuki Research Center, Nihon Bayer Agrochem K. K., Yuki, Ibaraki 307-0001, Japan

Received February 9, 1998; Revised Manuscript Received May 4, 1998

ABSTRACT: Scytalone dehydratase is a member of the group of enzymes involved in fungal melanin biosynthesis in a phytopathogenic fungus, *Pyricularia oryzae*, which causes rice blast disease. Carpropamid [(1*RS*,3*SR*)-2,2-dichloro-*N*-[(*R*)-1-(4-chlorophenyl)ethyl]-1-ethyl-3-methylcyclopropanecarboxamide] is a tight-binding inhibitor of the enzyme. To clarify the structural basis for tight-binding inhibition, the crystal structure of the enzyme complexed with carpropamid was analyzed using diffraction data collected at 100 K. The structural model was refined to a crystallographic *R*-factor of 0.180 against reflections up to a resolution of 2.1 Å. Carpropamid was bound in a hydrophobic cavity of the enzyme. Three types of interactions appeared to contribute to the binding. (i) A hydrogen bond was formed between a chloride atom in the dichloromethylethylcyclopropane ring of carpropamid and Asn-131 of the enzyme. (ii) The (chlorophenyl)ethyl group of carpropamid built strong contacts with Val-75, and this group further formed a cluster of aromatic rings together with four aromatic residues in the enzyme (Tyr-50, Phe-53, Phe-158, and Phe-162). (iii) Two hydration water molecules bound to the carboxamide group of carpropamid, and they were further hydrogen-bonded to Tyr-30, Tyr-50, His-85, and His-110. As a result of interactions between carpropamid and the phenylalanine residues (Phe-158 and Phe-162) in the C-terminal region of the enzyme, the C-terminal region completely covered the inhibitor, ensuring its localization in the cavity.

Rice blast disease is one of the most serious and damaging diseases in rice production. The disease is caused by a filamentous fungus, *Pyricularia oryzae* (teleomorph, *Magnaporthe grisea*). The pathogenic fungus directly penetrates into the rice plant from a cellular structure called an appressorium that is formed at the tip of the germ tube (*1*). Fungal melanin is synthesized through the polyketide pathway (*2*) and is arranged into a layer structure between the cell wall and the cell membrane of the appressorium. The melanin layer is a prerequisite for maintaining the structure of the appressorium against osmotic pressures as high as 8 MPa produced inside the appressorium. The fungus mechanically punctures the hard epidermis of rice by utilizing osmotic pressure and penetrates into rice. Thus, melanization of the appressorium is essential for pathogenic virulence, and the enzymes involved in the biosynthesis pathway of fungal melanin are good targets for developing control agents against rice blast disease.

Carpropamid [(1*RS*,3*SR*)-2,2-dichloro-*N*-[(*R*)-1-(4-chlorophenyl)ethyl]-1-ethyl-3-methylcyclopropanecarboxamide] was developed as a potent control agent against rice blast disease (*3*, *4*). Recent biochemical studies revealed that carpropamid strongly inhibits scytalone dehydratase (SDH)[1] (*5*), a member of the group of enzymes involved in melanin biosynthesis. SDH catalyzes two reaction steps in melanin biosynthesis: the conversion of scytalone to 1,3,8-trihydroxynaphthalene and the conversion of vermelone to 1,8-dihydroxynaphthalene (*6*). Carpropamid specifically binds to SDH (*5*) and inhibits the dehydration steps (*7*). A detailed kinetic study of the inhibition has shown that carpropamid works as a tight-binding inhibitor (*5*). The dissociation constant for carpropamid (K_i) was measured to be 0.14 nM and was about 2×10^5 times smaller than that for the substrate, scytalone ($K_m = 31\ \mu M$).

SDH is a soluble enzyme with an M_r of 20K consisting of 172 amino acid residues. The enzyme has a unique fold consisting of an $\alpha + \beta$ barrel motif and forms a trimer as shown by X-ray crystal structure analysis for the complex of (*R*)-(+)-*N*-[1-(4-bromophenyl)ethyl]-5-fluorosalicylamide

[†] This work was supported in part by grants for the Special Postdoctoral Researchers Program, for the Biodesign Research Program, for the SR Structural Biology Research Program, and for Promotion of Research from RIKEN. This work was also supported by Grants-in-Aid for Scientific Research from the Ministry of Education, Science, Sports and Culture of Japan (08272236).

[‡] This structure has been deposited in the Brookhaven Protein Data Bank under file name 2STD.

* To whom correspondence should be addressed. Telephone: (81)-48-467-9516. Fax: (81)-48-462-4676.

[§] Japan Science and Technology Corp. and The University of Tokyo.

[∥] The Institute of Physical and Chemical Research.

[⊥] Nihon Bayer Agrochem K. K.

[1] Abbreviations: SDH, scytalone dehydratase; BFS, (*R*)-(+)-*N*-[1-(4-bromophenyl)ethyl]-5-fluorosalicylamide; PEG, poly(ethylene glycol); rms, root-mean-square.

S0006-2960(98)00321-3 CCC: $15.00
Published on Web 06/19/1998

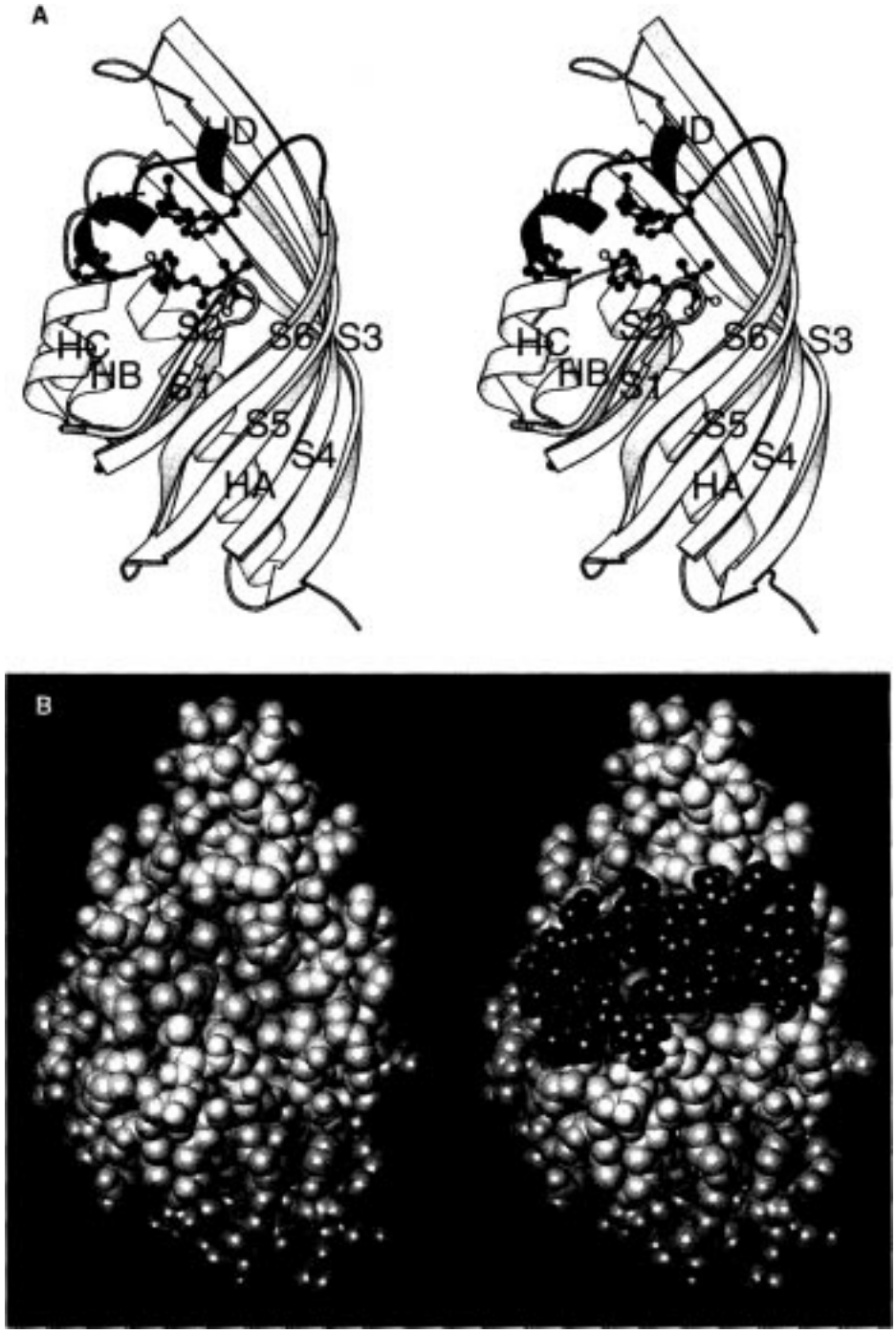

FIGURE 1: (A) Stereoplot of a ribbon model illustrating the structure of SDH complexed with carpropamid. The main body of SDH is colored in yellow, and the C-terminal region (residues 152−170) is colored in red. Carpropamid and three phenylalanines in the C-terminal region (Phe-158, Phe-162, and Phe-169) are shown as a ball-and-stick model. (B) CPK representations of the SDH−carpropamid complex (right) viewed from nearly the same orientation depicted in panel A. The structure at the left is the same as the right panel except the C-terminal region (residues 152−170) is removed from SDH. Carpropamid is gray; otherwise, the same colors are used as are used in panel A. The ribbon model in panel A was drawn with MOLSCRIPT (*24*).

(BFS) and SDH (*9*). SDH has a hydrophobic cavity where substrates bind. About 20 residues in the C-terminal region covering the binding pocket are thought to function as a lid for the cavity.

To clarify the structural basis for tight-binding inhibition by carpropamid, we determined the crystal structure of the complex of SDH and carpropamid by cryogenic X-ray crystallography. Here, we describe the structural basis of tight-binding inhibition and discuss the role of the C-terminal region in the binding of substrates and inhibitors.

MATERIALS AND METHODS

Crystallization of the Complex of SDH and Carpropamid. A recombinant SDH was produced using an *Escherichia coli* overexpression system and was purified as described previously (*8*). Carpropamid was synthesized as reported (*4*). Before each crystallization trial, 1 mg of SDH and 0.17 mg of carpropamid were mixed in a 40 mL solution of 10 mM TES (pH 7.0) and the mixture was incubated for 2 days at 4 °C. The resulting solution was concentrated to 16 mg/

mL SDH by ultrafiltration. All the crystallization trials were carried out with the hanging drop vapor diffusion method at 20 °C. Crystallization of the complex was achieved by poly(ethylene glycol) (PEG) 3350 (Sigma) in a relatively narrow pH range (±0.2) with an optimum at pH 5.2. The precipitant solution contained 14.5% (w/v) PEG 3350, 280 mM ammonium sulfate, and 200 mM sodium acetate. The crystals had a thin hexagonal plate shape, and the dimensions of the crystals were typically 0.35 mm wide and 0.08 mm thick. The crystal belonged to the space group *P*321, and the lattice constants were as follows: $a = 74.54$ Å, $b = 74.54$ Å, and $c = 71.20$ Å. One subunit of SDH was contained in an asymmetric unit, and the solvent content of the crystal was calculated to be 65%. The obtained crystal was nearly isomorphous with that of the BFS−SDH complex (*9*).

Cryogenic X-ray Diffraction Data Collection. Cryogenic X-ray diffraction experiments were performed by the oscillation method at 100 K. In the experiments, a R-Axis IV system (Rigaku), double-mirror focusing optics (Rigaku), and a rotating anode type X-ray generator (Ultrax18, Rigaku) were used. In cryogenic experiments, protein crystals were rapidly and continuously cooled with a cold nitrogen gas generator (Rigaku). The exit nozzle of the generator was placed within 10 mm of a crystal, and the temperature of the gas was adjusted to 100 K at the sample position with a thermocouple. The X-ray generator was operated at a load of 3.6 kW (45 kV and 80 mA), and the focus size was 0.3 mm × 3 mm. CuKα radiation (=1.5418 Å) was selected with a Ni foil that was 10 μm thick. The crystal−detector distance was set to 150 mm. For crystal mounting in the cryogenic experiment, an original crystal mounting device was used (*10*).

Before cryogenic experiments, the mother liquor of the crystal was exchanged to a cryoprotectant solution. The harvested crystals were transferred into a microdialysis cell and were dialyzed against a cryoprotectant solution containing 25% (w/v) PEG 3350, 30% (w/v) sucrose, 280 mM ammonium sulfate, and 200 mM sodium acetate (pH 5.2). No crystals were cracked or dissolved after dialysis for 12 h.

Diffraction data were collected up to 2.1 Å resolution as a series of 1.5° oscillation frames with an exposure time of 15 min. The indexing of reflections, the calculation of integrated intensities, scaling, and postrefinement were performed with the program PROCESS in the R-axis IV system. The absorption effect originating from the cryoprotectant solution remaining in the mounting device was corrected in the scaling process with the program SCCRYO (M. Nakasako, unpublished results). A total of 50 287 reflections were measured between 20.0 and 2.1 Å, and the overall $R_{\mathrm{merge}}{}^{I}$ [$=\Sigma_{hkl}\Sigma_i|I_i(hkl) - \langle I(hkl)\rangle|/\Sigma_{hkl}\Sigma_i I_i(hkl)$] was 0.073 for the symmetry-related reflections. The number of unique reflections was 12 014, corresponding to a completeness of 85.6%. The completeness in the highest-resolution shell between 2.2 and 2.1 Å was 74.6%.

Structure Refinement and Model Building. Structure refinement was carried out with X-PLOR (*11*) followed by model building with turbo FRODO (BIO-GRAPHICS). Because the present crystal was nearly isomorphous with that of the crystal of the BFS−SDH complex, the coordinates of the BFS−SDH complex (*9*) were used as the starting model of the structure refinement [the crystal structure of the BFS−SDH complex has been registered as 1STD in the Brookhaven Protein Data Bank (*12*)]. A rigid-body refinement was applied for moving the initial model to a correct position relative to the crystal lattice using the amplitude data between 8.0 and 3.5 Å resolution. After the rigid-body refinement, the crystallographic *R*-factor [$R = \Sigma_{hkl}|F_{\mathrm{obs}}(hkl) - F_{\mathrm{calc}}(hkl)|/\Sigma_{hkl}F_{\mathrm{obs}}(hkl)$] of the resultant model was 0.31. The conventional refinement procedures followed by model building were then iterated. At the early stage of the structure refinement, the residues in the C-terminal region of the starting model (from 152 to 170) were removed because the initial model was not consistent even with the calculated $2F_o - F_c$ electron density maps. The C-terminal region was finally reconstructed with $F_o - F_c$ difference Fourier maps. Hydration water molecules were picked up with a suite of FESTKOP programs (M. Nakasako, unpublished results). Newly introduced residues or hydration water molecules were examined after the subsequent refinement with omit-annealed $F_o - F_c$ difference Fourier maps.

The final structural model contained 1377 non-hydrogen atoms of the enzyme, one carpropamid molecule, one sulfate

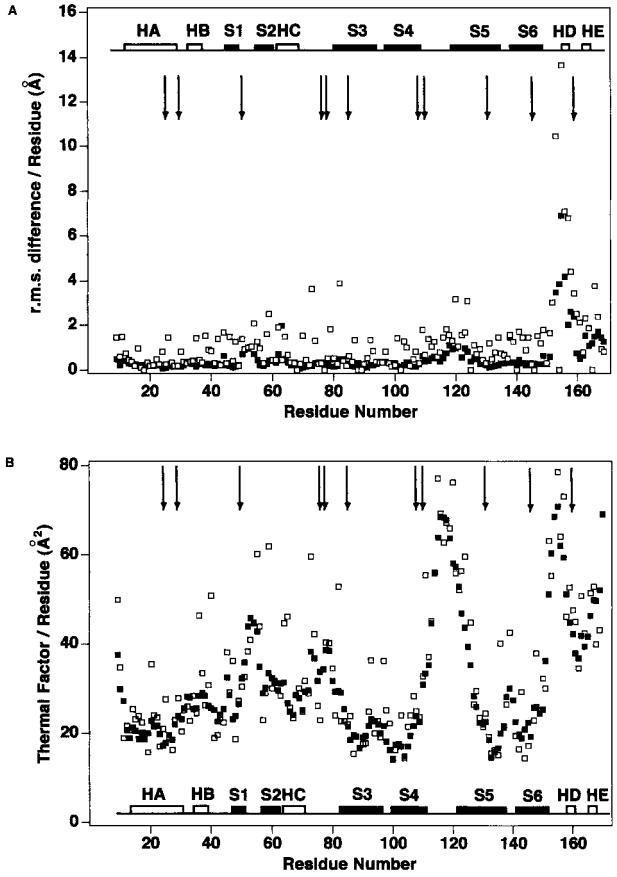

FIGURE 2: (A) The rms differences in backbone and side chain atoms between SDHs in the carpropamid−SDH and BFS−SDH complexes are plotted against residue number. Full squares represent differences in backbone atoms and open ones those in side chain atoms. The rms differences were calculated after superimposing the main bodies of SDHs in the two models by least-squares calculation for the main chain atoms in the secondary structures HA−C and S3−6. (B) Average temperature factors of residues in SDH plotted against the residue number. The filled and open squares represent the values for main chain atoms and side chain atoms, respectively. The secondary structures, α-helices (open boxes), β-strands (filled boxes), and loops (lines), are specified in the figures. The arrows indicate the residues that form the hydrophobic cavity in SDH.

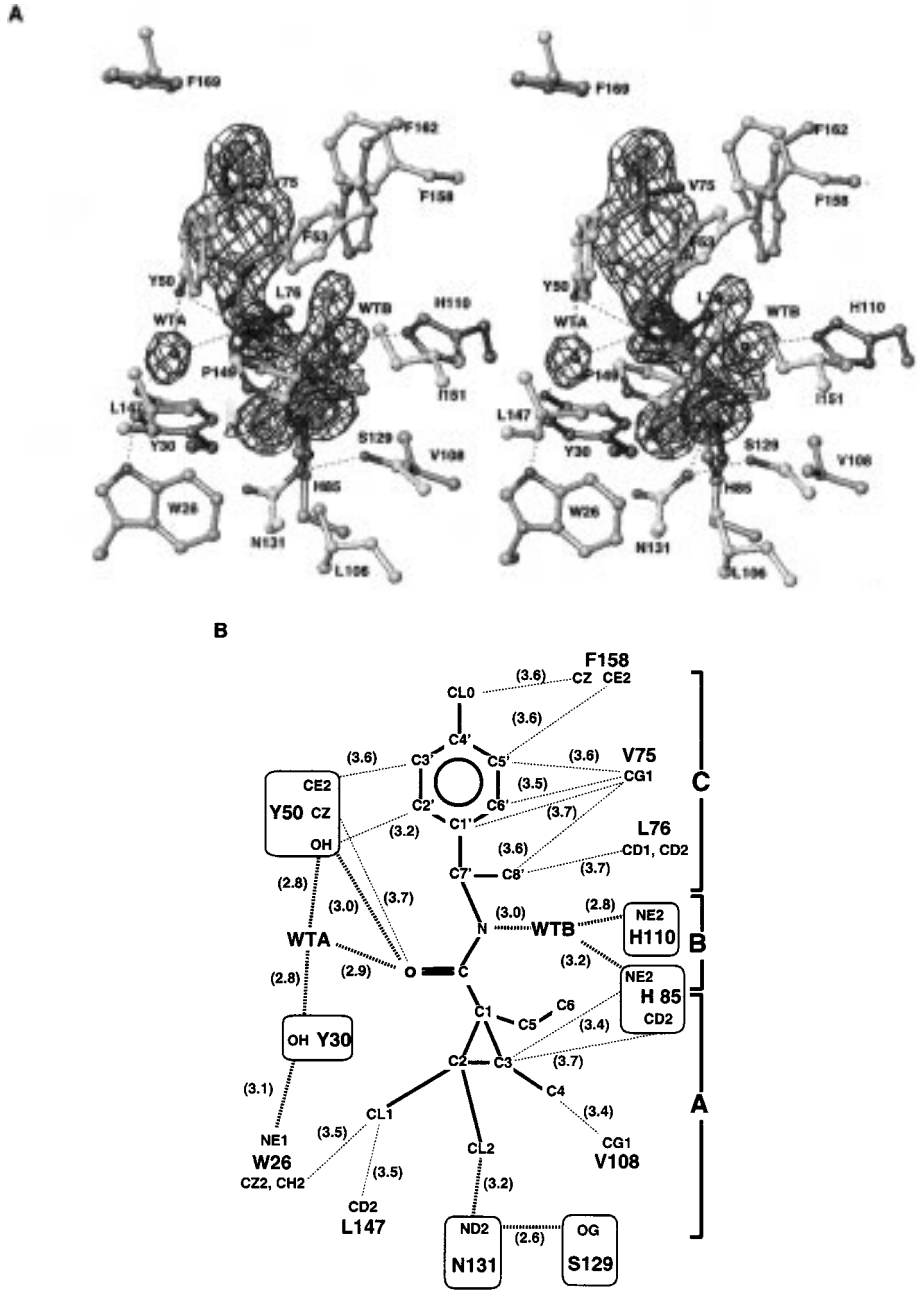

FIGURE 3: (A) Stereoplot of an omit $F_o - F_c$ difference Fourier map for carpropamid and two hydration waters bound to the carboxamide group. Also shown are the side chains forming the hydrophobic cavity (represented with a ball-and-stick model). The reflections between 8.0 and 2.1 Å resolution were used for the calculation of the map. The blue and pink fishnets are drawn in 3.2 and 8.0 standard deviations of the map, respectively. The hydrogen bonds important for stabilizing carpropamid in the cavity are shown with orange dashed lines. Each residue is identified with the one-letter code and the residue number. (B) A schematic drawing of the interactions between carpropamid and SDH. Figures in parentheses represent the distances between two atoms engaged in the interaction. Hydrogen bonds and van der Waals interactions are represented by thick and thin dotted lines, respectively. The hydrophilic residues are boxed. A−C represent the structural segments of carpropamid.

ion, and 174 hydration water molecules. For the 11 759 unique reflections [$F/\sigma(F) > 2.0$] between 8.0 and 2.1 Å resolution, the model gave a crystallographic *R*-factor of 0.179 (for 90% of the unique reflections) and an R_{free} of 0.259 (for the remaining 10% of the unique reflections). The mean positional error of atoms in the final structural model was estimated to be 0.22 Å using Luzzati's method (*12*). The root-mean-square (rms) deviations from the ideal case were 0.010 Å for bond lengths and 1.72° for bond angles.

RESULTS

Structure of SDH Complexed with Carpropamid. Confirming the previous results (*9*), we found the main body of SDH (residues 9−151) consisted of three α-helices (HA−C), six β-strands (S1−6), and loops connecting those secondary structures (Figure 1A). The model for the C-terminal region (residues 152−170) was rebuilt as two short helices (HD and HE) and three loop structures (see Materials and Methods). The final model did not include the eight N-terminal residues and two C-terminal residues because of poor electron densities for these residues. The inhibitor, carpropamid, was located in a cavity formed by the residues from all the β-strands and the four α-helices (HA and HC−E) (Figure 1A). Carpropamid was covered by the C-terminal region that would serve as a lid for the

Table 1: Dihedral Angles Determining the Conformation of Carpropamid in the Hydrophobic Cavity of SDH[a]

target	dihedral angle (deg)
C2−C1−C5−C6	173.2
C2−C1−C−O	53.4
C−N−C7−C1	86.1
N−C7−C1′−C2′	53.2

[a] The atoms are identified in Figure 3B.

cavity (Figure 1B). The rms differences between SDHs in the carpropamid−SDH and the BFS−SDH complexes were 0.31 Å for the α-carbon atoms of HA−C and S3−6 composing the main bocy of SDH (Figure 2A). In contrast with the main body of SDH, the structures in the C-terminal region were remarkably different between SDHs in the two complexes (Figure 2A). Even at 100 K, thermal factors were extremely large for the residues in the loop between S4 and S5 and another loop between S6 and HD (Figure 2B).

Structure of Carpropamid Confined in SDH. The conformation of the inhibitor, carpropamid, was obvious from the well-defined difference Fourier map shown in Figure 3A. For instance, the three chloride atoms and the cyclopropane ring of carpropamid were easily assigned by increasing the contour level of the density map (purple fishnet in Figure 3A). Carpropamid was positioned in the hydrophobic cavity so that the dichloroethylmethylcyclopropane group interacted with the bottom of the pocket composed of the residues from S4−6; the (chlorophenyl)ethyl group at the opposite end of the inhibitor pointed toward helix HE (Figure 1A). The dihedral angles specifying the conformation of carpropamid in the cavity were tabulated in Table 1.

Interactions between Carpropamid and the Amino Acid Residues Forming the Cavity. Carpropamid was confined in the cavity formed by the 20 amino acid residues, namely, Trp-26, Tyr-30, Tyr-50, Phe-53, Leu-54, Met-69, Val-75, Leu-76, Thr-83, His-85, Val-108, His-110, Ala-127, Asn-131, Leu-147, Pro-149, Ile-151, Phe-158, Phe-162, and Phe-169. About two-thirds of these residues are hydrophobic. In particular, the three phenylalanine residues (158, 162, and 169) in the C-terminal region were engaged in the formation of the cavity despite their large thermal factors (Figures 1A, 2B, and 3A). Two well-ordered hydration water molecules (WTA and WTB in Figure 3) were bound to the carboxamide group of the inhibitor. Direct interactions between carpropamid and SDH consisted of two hydrogen bond (<3.4 Å) and 43 van der Waals contacts (<4 Å). Major interactions are illustrated in Figure 3B. The structure of the inhibitor can be thought to consist of three segments: dichloroethylmethylcyclopropane (A), carboxamide (B), and (chlorophenyl)ethyl (C) groups. The characteristics of the interactions vary accordingly.

In region A, one hydrogen bond and 17 van der Waals interactions (<4 Å) were observed. The CL2 atom of carpropamid and the ND2 atom of Asn-131 formed a hydrogen bond. The direction of this bond was fixed by the hydrogen bond between ND2 of Asn-131 and OG of Ser-129. The thermal factors of these two residues were the lowest in all the residues forming the cavity (Figure 2B). The orientation of the cyclopropane ring was determined by the five van der Waals contacts with Trp-26, His-85, Val-108, and Leu-147. The CL1 atom may have contributed to the binding through electrostatic interactions with partial charges of Leu-147 and Trp-26.

Table 2: Centroid Distances and Dihedral Angles between Aromatic Rings in Regions A and B in Figure 3[a]

residue	residue	centroid distance (Å)	dihedral angle (deg)
Tyr-50	carpropamid	5.5	87
Phe-53	carpropamid	6.8	88
Phe-158	carpropamid	6.0	60
Phe-162	carpropamid	5.1	88
Phe-169	carpropamid	7.0	80
Phe-53	Phe-158	5.2	64
Trp-153	Phe-158	6.4	68
Phe-158	Phe-162	5.7	54

[a] Only the pairs whose centroid distance is within 7 Å are listed.

In region B, two well-ordered hydration water molecules were bound to the carboxamide group of carpropamid (Figure 3A). The hydration water molecules formed four hydrogen bonds with hydrophilic residues of the enzyme (His-85, His-110, Tyr-30, and Tyr-50). In region B, the carboxamide group of the inhibitor was fixed by these interactions and one hydrogen bond with Tyr-50. The distances and the angles of hydrogen bonds formed by hydration waters were very similar to those in the ideal hydrogen bond. Thus, these two hydration water molecules can fix the carboxamide group of the inhibitor in the central region of the cavity, although there is one direct hydrogen bond between carpropamid and the enzyme.

In region C, 26 van der Waals interactions (<4 Å) were observed. The (chlorophenyl)ethyl group of carpropamid strongly interacted with the enzyme through nine van der Waals interactions with Tyr-50, Val-75, Leu-76, and Phe-158 (Figure 3B). The van der Waals interactions between carpropamid and two hydrophobic residues (Val-75 and Leu-76) were so strong that the main chain of Val-75 was largely distorted into an unfavorable conformation; the main chain torsion angles of Val-75, ϕ and φ, were −129 and −113°, respectively. This distortion indicates that the binding of carpropamid might have caused a change in the secondary structure of a segment (Lys-73−Gly-77) following helix HC.

The (chlorophenyl)ethyl group formed a cluster of aromatic rings together with the side chains of Tyr-50, Phe-53, Phe-158, and Phe-162. Table 2 lists the centroid distances and dihedral angles between those phenyl rings that characterize the arrangement of the aromatic rings. In particular, the planes of the phenyl rings of Phe-162 and Tyr-50 were nearly perpendicular to the plane of the chlorophenyl group and were very close (<6 Å) to being favorable for aromatic−aromatic interactions (*14*). Furthermore, these two aromatic rings were symmetrically located against the chlorophenyl group of carpropamid, efficient for determining the orientation of the chlorophenyl ring in region C. Of the four aromatic residues forming the cluster, Phe-158 and Tyr-50 were located close to the (chlorophenyl)ethyl group and formed eight van der Waals contacts (<4 Å) with the group. As a result of this close packing, the cavity in region C was narrower than those in regions A and B, presumably helping the inhibitor confined in the cavity.

Structure of the C-Terminal Region. A structural model for the C-terminal region (residues 152−170) was built independently from the former model (*9*) on the basis of the

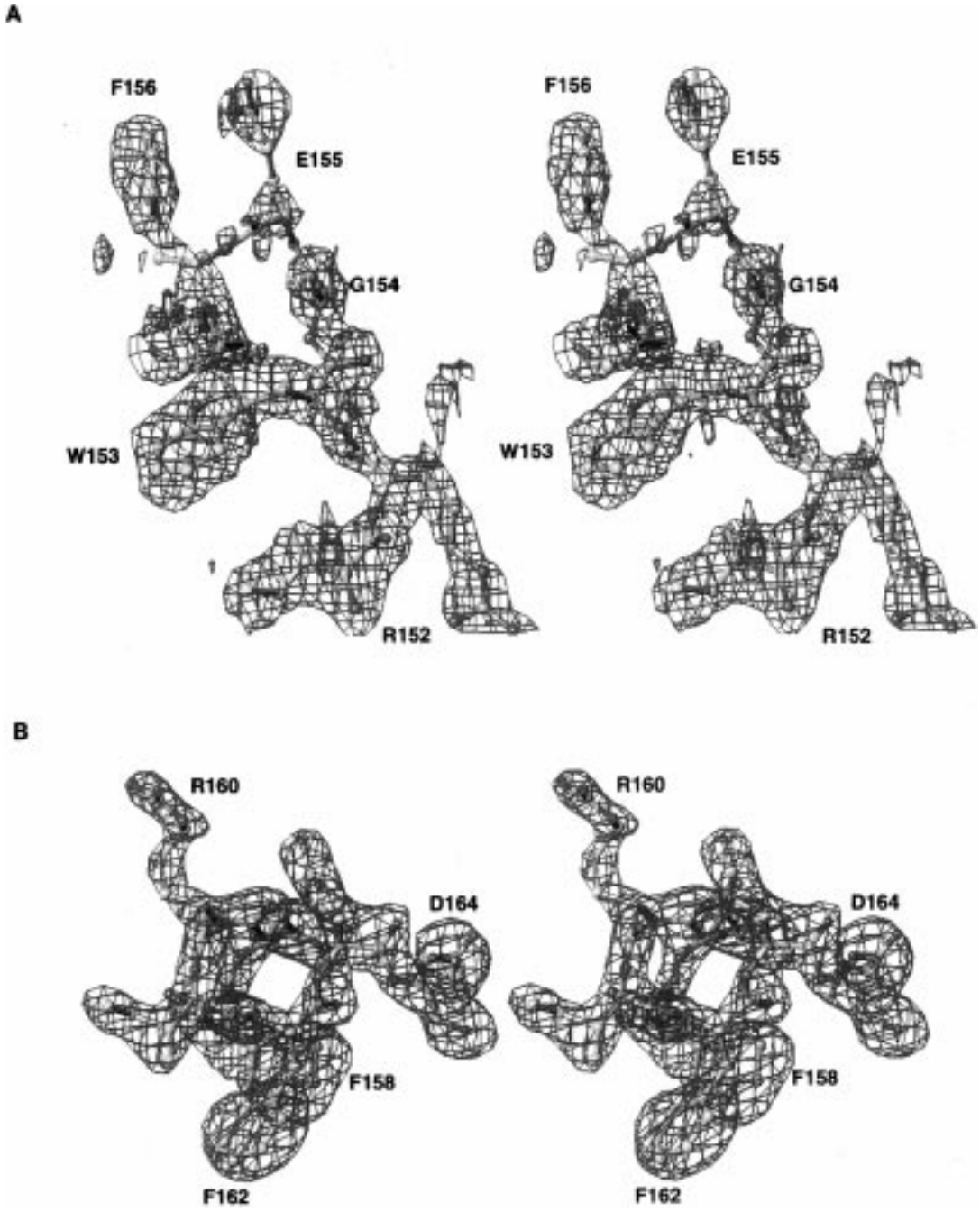

FIGURE 4: Omit $F_o - F_c$ difference Fourier maps for the residues of the C-terminal region. The maps were calculated with the diffraction amplitude data between 8.0 and 2.1 Å resolution. Blue fishnets represent 2.5 and 3.0 standard deviations of the maps in panels A and B, respectively. The residues are represented in the same way as they are in Figure 3A. (A) The map for the linker loop having high positional fluctuation between S6 and HD, namely, Ile-151, Arg-152, Trp-153, Gly-154, Glu-155, and Phe-156. (B) The map for Phe-158, Asp-159, Arg-160, Ile-161, Phe-162, Glu-163, and Asp-164.

electron density maps shown in Figure 4. The present model for the region was composed of two short helices [HD (158−161) and HE (165−168)], three loops (152−157, 162−164, and 169−170) and nine hydration water molecules (X01−5, X10, X11, WT1, and WT2) (Figures 1A and 5). The characteristic structure of the C-terminal region seemed to be stabilized by hydrogen bonds mediated by these hydration water molecules and nonbonded interactions between carpropamid and phenylalanine residues in the region.

Five hydration water molecules (X01−5) contributed greatly to the determination of the structure of the C-terminal region, in that 12 of 20 hydrogen bonds (<3.4 Å) within the C-terminal region were formed by those hydration water molecules. In particular, hydration water molecules X01 and X04 were important in determining the orientations of the two short helices, HD and HE. The hydration water molecules formed a network of hydrogen bonds that linked the Asp-159 in HD and Arg-166 and Glu-167 in HE. Then, the principal axes of the two short helices were set to be nearly perpendicular by the network. Three hydration water molecules, X02, X03, and X05, also contributed to the stabilization of the C-terminal region by forming hydrogen bonds within certain residues or between adjoining residues.

Direct interactions between the C-terminal region and the main body of SDH were relatively weak. The C-terminal region formed three van der Waals contacts with the side

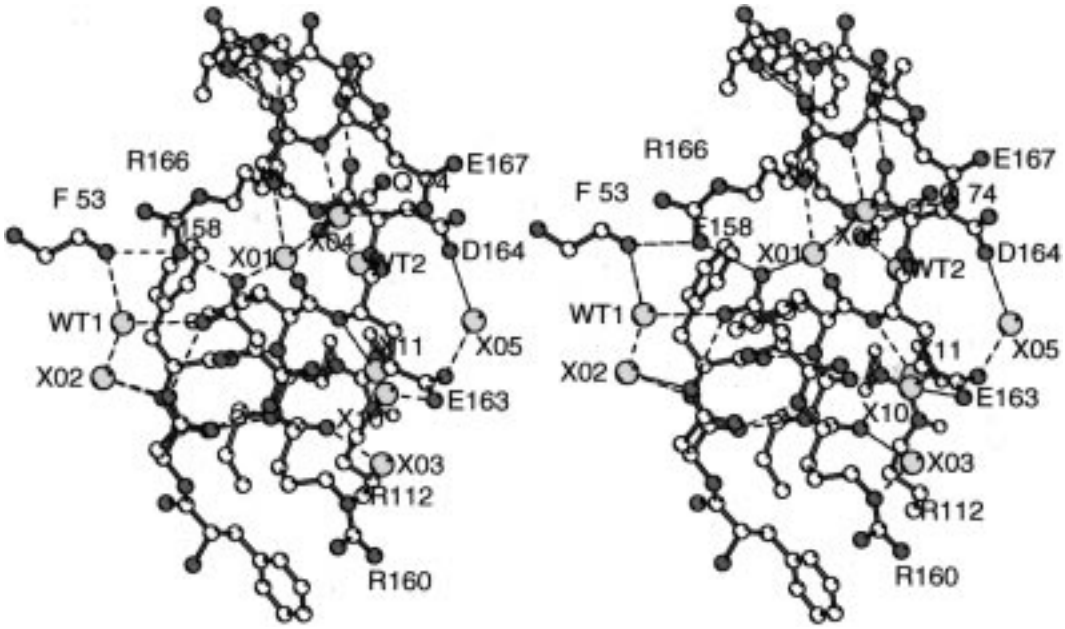

FIGURE 5: Stereoplot of the ball-and-stick model for a part of the C-terminal region (residues 156−170) viewed from outside. The residues from the main body of SDH interacting with the C-terminal region via hydrogen bonds are also shown. The red, blue, and yellow spheres represent oxygen atoms, nitrogen atoms, and hydration waters, respectively. The hydrogen bonds are shown with dashed lines. The notations for hydration waters are divided into two groups. WT represents those mediating the interactions between the C-terminal region and the main body of SDH and X those stabilizing the C-terminal region. This figure was drawn with MOLSCRIPT (*24*).

chains from S2 and S5. There were only two direct hydrogen bonds with Arg-112 and Phe-53 and two loose links mediated by hydration water molecules (WT1 and WT2) between the C-terminal region and the main body of SDH. The large thermal fluctuation of the C-terminal region (Figure 2B) might be ascribed to this lack of strong interactions.

The C-terminal region interacted with carpropamid through the aromatic−aromatic interactions and van der Waals contacts through the three phenylalanine residues (Phe-158, Phe-162, and Phe-169) (Table 2 and Figure 3B). Because carpropamid strongly bound to the main body of the SDH as described in the previous section, these interactions indirectly fixed the C-terminal region to the main body of SDH.

DISCUSSION

A cryogenic crystal structure analysis at 2.1 Å resolution unambiguously revealed various types of interactions that would cause the tight-binding inhibition by carpropamid to SDH (Figure 3B). Here, we discuss the structural bases for the tight-binding inhibition by carpropamid to SDH and the role of the C-terminal region in the binding of inhibitors or substrates.

Structural Basis of Tight-Binding Inhibition. The hydrogen bond between the CL2 atom in the dichloroethylmethylcyclopropane group and the NE2 atom of Asn-131 (Figure 3) is one of the determining factors in tight-binding inhibition. The importance of the dichlorocyclopropane group has been recognized in the process of developing carpropamid (*4*). In the competitive inhibitor BFS [(*R*)-(+)-*N*-[1-(4-bromophenyl)ethyl]-5-fluorosalicylamid], region A contains a fluorosalicylamide group (*9*) (Figure 6A). A hydrogen bond formed between the OH of this group in BFS and Asn-131 would be weaker than the hydrogen bond in the carpropamid−SDH complex.

The ethyl group (C5 and C6 in Figure 3B) in region A of carpropamid is also important in tight-binding inhibition. The presence of the group caused a remarkable structural difference between the cavities of the carpropamid−SDH complex and that of BFS−SDH; Phe-158 in the carpropamid−SDH complex moved more than 4 Å from the relative position in the BFS−SDH complex because of steric hindrance with the ethyl group (Figures 2A and 6A). The positional change of Phe-158 induced several interactions that were favorable to tight-binding inhibition. Strong interactions between Phe-158 and the CL0 atom of the (chlorophenyl)ethyl group (Figure 3B) should contribute to tight-binding inhibition, because phenylethyl groups decorated with a single halogen atom (Cl or Br) have been shown to be required for increasing antifungal efficacy of control agents (*4*). The change increased the stability of the cluster of aromatic rings in region C (Table 2) and induced 15 van der Waals interactions (<4 Å) between carpropamid and the aromatic rings. Simultaneously, a large positional change of Trp-153 occurred in the linker region between S6 and HD (Figures 2A and 6B). Trp-153 indirectly contributed to stabilization of the aromatic cluster in the carpropamid−SDH complex (Table 2). The positional change of Phe-158 also caused a narrowing in the upper region of the hydrophobic cavity, thus inhibiting the dissociation of carpropamid from SDH.

The carboxamide group is also one of the structural elements required for effective inhibition with respect to SDH. Because four of five hydrogen bonds observed in region B were afforded by two hydration water molecules (WTA and WTB in Figure 3), hydration of the group is considered to be an important factor in fixing the group in the cavity. The importance of this group has been demonstrated by a kinetic study on salicylamide (*15*); the deletion of carbonyl oxygen from the inhibitor drastically reduced the degree of inhibition.

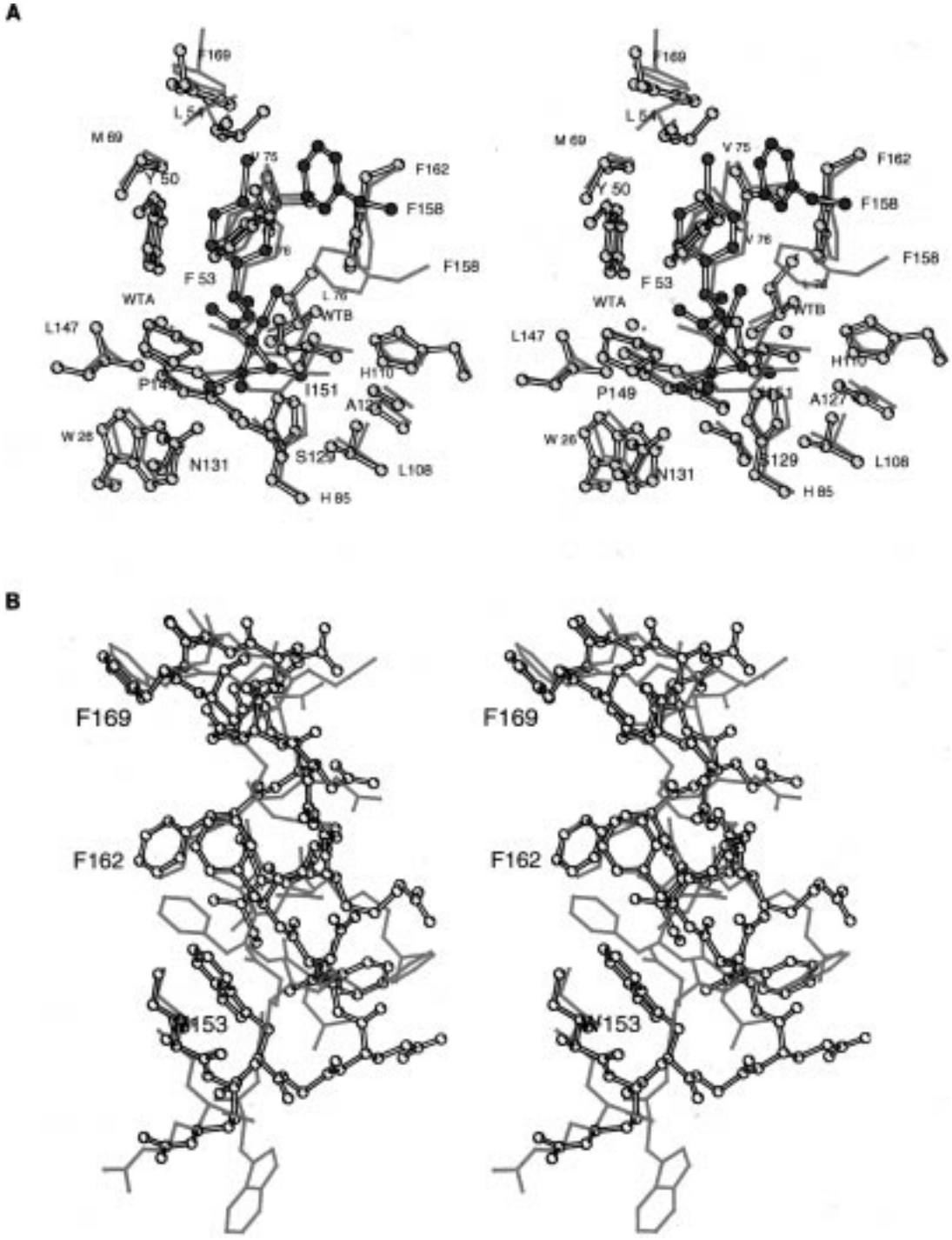

FIGURE 6: (A) Structures of the binding cavity and inhibitors in the carpropamid−SDH (represented with a ball-and-stick model) and the BFS−SDH (drawn with a wire model colored in red) complexes. In the carpropamid−SDH model, atoms in the carpropamid molecule and the side chain of Phe-158 are colored in blue and green, respectively. (B) Structures of the C-terminal region (residues 152−170) in the carpropamid−SDH and BFS−SDH complexes. Models are represented in the same way as they are in panel A except for the color of the atoms of Phe-158. These figures were drawn after superimposing the main bodies of SDHs in the two models by least-squares calculation for the main chain atoms in the secondary structures HA−C and S3−6. These figures were drawn with MOLSCRIPT (*24*).

In summary, we propose the following structural bases for tight-binding inhibition of carpropamid. (i) The chloride atom, CL2, in the dichloromethylethylcyclopropane group forms a hydrogen bond with Asn-131 in region A. (ii) The (chlorophenyl)ethyl group makes a tight contact with helix HC and four aromatic residues in region C. (iii) The ethyl group decorating the cyclopropane group causes a rearrangement of Phe-158 so that the cluster of aromatic rings in region C is stabilized and the cavity in region C is narrowed. (iv) The carboxamide group and two hydration water molecules form hydrogen bonds in region B. These structural bases revealed by our structural analysis should prove useful in designing efficient and novel inhibitors for SDH.

Structural bases similar to those observed in the carpropamid−SDH complex have been found in inhibitor−enzyme or hapten−Fab fragment complexes. For instance, a tight-binding inhibitor for aldose reductase, zopolrestat, has three fluorine atoms and two aromatic rings, greatly contributing

to its binding affinity (*16*−*18*). Synthetic peptides inhibiting aspartic proteinase have their affinities drastically increased when they are decorated with several aromatic rings to form an aromatic cluster in the binding site (*19*). The formation of clusters of aromatic rings has also been observed in complexes of various haptens and Fab fragments of immunoglobulins (*20*−*23*). Thus, some of the structural bases observed in the carpropamid−SDH complex may become common factors in designing novel agents for targeting enzymes or proteins.

Structure of the Flexible C-Terminal Region. The structure of the C-terminal region of SDH in the carpropamid−SDH complex was quite different from that in the BFS−SDH complex (Figures 2A and 6B). The length of helix HD was half of that in the BFS−SDH complex, and large positional changes occurred in Trp-153 and Phe-158. These structural changes and the thermal fluctuation of the C-terminal region (Figure 2B) suggest that the C-terminal region, particularly the residues from 152 to 159, is extremely flexible and can be deformed easily by inhibitors. In the binding of substrates or inhibitors, SDH must move the C-terminal region to expose its hydrophobic cavity to solvent. In that motion, the loop linking S6 and HD may work as a hinge as has been observed for several proteins showing large structural changes upon binding of substrates or inhibitors (*24*).

Phe-162 occupied corresponding positions in carpropamid−SDH and BFS−SDH complexes, despite the large structural differences in the residues from 152 to 158 (Figure 6). This fact suggests that the phenylalanine residue is important in the binding of inhibitors or substrates. A surprising result of mutagenesis experiments involving SDH (*5*) indicates that deletion of Phe-162 causes the loss of SDH enzymatic activity. Furthermore, even a point mutation of Phe-162 to alanine causes this loss of activity (T. Motoyama et al., in preparation). Thus, the phenylalanine residue not only helps to stabilize the bulky inhibitor in the cavity but also is crucial for preserving enzymatic activity.

The size of the substrate, scytalone, is half of that of carpropamid and the enzymatic reaction occurs in the "A" and the "B" regions as proposed (*9*). Thereafter, the substrate must be confined in the bottom area of the cavity. The phenylalanine residue may work like a tentacle, driving the substrate into the bottom of the cavity. During this process, a large conformational change would occur in the C-terminal region. To refine this model for substrate recognition by SDH, further studies need to be carried out at the molecular level.

ACKNOWLEDGMENT

We thank Drs. T. Iizuka (RIKEN), I. Ueyama (Nihon Bayer Agrochem Co.), and S. Kagabu (Gifu University) for their fruitful discussions and comments about this work. We acknowledge Prof. C. Toyoshima (The University of Tokyo) and Dr. M. Schindler (Bayer A.G.) for critical reading of the manuscript.

REFERENCES

1. Yamaguchi, I., and Kubo, Y. (1992) in *Target sites of fungicide action*, pp 101−118, CRC Press, London.
2. Bell, A. A., and Wheeler, M. H. (1986) *Annu. Rev. Phytopathol. 24*, 411−415.
3. Hattori, T., Kurahashi, Y., Kozine, T., and Kagabu, S. (1994) *Brighton Crop Prot. Conf. Proc. 2*, 517−524.
4. Kagabu, S., and Kurahashi, Y. (1998) *J. Pestic. Sci. 23*, 145−147.
5. Motoyama, T., Imanishi, K., Kinbara, T., Kurahashi, Y., and Yamaguchi, I. (1998) *J. Pestic. Sci. 23*, 58−61.
6. Butler, M. J., Lazarovits, G. L., Higgins, V. J., and Lachance, M.-A. (1988) *Exp. Mycol. 12*, 357−376.
7. Kurahashi, Y., Sakawa, S., Kinbara, T., Tanaka, K., and Kagabu, S. (1997) *J. Pestic. Sci. 22*, 108−112.
8. Motoyama, T., Imahashi, K., and Yamaguchi, I. (1998) *Biosci., Biotechnol., Biochem. 62*, 564−566.
9. Lundquist, T., Rice, J., Hodge, C. N., Basarab, G. S., Pierce, J., and Lindqvist, Y. (1994) *Structure 2*, 937−944.
10. Nakasako, M., Ueki, T., Toyoshima, C., and Umeda, Y. (1995) *J. Appl. Crystallogr. 28*, 856−857.
11. Brünger, A. T. (1992) *X-PLOR Version 3.1. A System for X-ray Crystallography and NMR*, Yale University Press, New Haven, CT.
12. Bernstein, F. C., Koetzle, T. F., Williams, G. J. B., Meyer, E. F., Brice, M. D., Rodgers, J. R., Jr., Kennard, O., Shimanouchi, T., and Tasumi, M. (1977) *J. Mol. Biol. 112*, 535−542.
13. Luzzati, P. V. (1952) *Acta Crystallogr. 5*, 802−810.
14. Burley, S. K., and Petsko, G. A. (1986) *FEBS Lett. 203*, 139−143.
15. Hodge, C. N., and Pierce, J. (1993) *Bioorg. Med. Chem. Lett. 3*, 1605−1608.
16. Nakano, T., and Petrash, J. M. (1996) *Biochemistry 35*, 11196−11202.
17. Wilson, D. K., Tarle, I., Petrash, J. M., and Quiocho, F. A. (1993) *Proc. Natl. Acad. Sci. U.S.A. 90*, 9847−9851.
18. Wilson, D. K., Nakano, T., Petrash, J. M., and Quiocho, F. A. (1995) *Biochemistry 34*, 14323−14330.
19. Cutfield, S. M., Dodson, E. J., Anderson, B. F., Moody, P. C. E., Marshall, C. J., Sullivan, P. A., and Cutfield, J. F. (1995) *Structure 3*, 1261−1271.
20. Love, R. A., Villafranca, J. E., Aust, R. M., Kevin, K., Nakamura, K., Jue, R. A., Major, J. G., Jr., Radhakrishnan, R., and Butler, W. F. (1993) *Biochemistry 32*, 10950−10959.
21. Hsieh-Wilson, L., Schultz, P. G., and Stevens, R. C. (1996) *Proc. Natl. Acad. Sci. U.S.A. 93*, 5363−5367.
22. Mizutani, R., Miura, K., Nakayama, T., Shimada, I., Arata, Y., and Satow, Y. (1995) *J. Mol. Biol. 254*, 208−222.
23. Guddat, L. W., Shan, L., Anchin, J. M., Linthicum, D. S., and Edmundson, A. B. (1994) *J. Mol. Biol. 236*, 247−274.
24. Shulz, G. E. (1991) *Curr. Opin. Struct. Biol. 1*, 883−888.
25. Kraulis, P. J. (1991) *J. Appl. Crystallogr. 24*, 946−950.

BI980321B